Formation of diphenyl-bipyridine units by surface assisted cross coupling in Pd-cyclometalled complexes

Jose Eduardo Barcelon [a,b,1], Marija Stojkovska [a,c,1], Daniele Perilli [d], Giovanni Carraro [a], Marco Smerieri [a], Luca Vattuone [a,e], Mario Rocca [a,e], Gianangelo Bracco [a,e], Martina Dell'Angela [f], Roberto Costantini [f], Albano Cossaro [f,g], Luca Vaghi [d], Antonio Papagni [d], Cristiana Di Valentin [d,*], Letizia Savio [a,*]

[a] IMEM-CNR, UOS Genova, Via Dodecaneso 33, 16146 Genova, Italy
[b] Dipartimento di Scienze Chimiche, della Vita e della Sostenibilità Ambientale, Università di Parma, Parco Area delle Scienze, 17/A, 43124 Parma, Italy
[c] Dipartimento di Chimica, Università degli Studi di Genova, Via Dodecaneso 31, 16146 Genova, Italy
[d] Dipartimento di Scienza dei Materiali, Università di Milano-Bicocca, Via R. Cozzi 55, 20125 Milano, Italy
[e] Dipartimento di Fisica, Università degli Studi di Genova, Via Dodecaneso 33, 16146 Genova, Italy
[f] CNR-IOM, Strada Statale 14 – km 163.5, 34149 Trieste, Italy
[g] Dipartimento di Scienze Chimiche e Farmaceutiche, Università degli Studi di Trieste, via L. Giorgieri 1, 34127 Trieste, Italy

ARTICLE INFO

Keywords:
Cross coupling reactions
Pd cyclometallated compounds
Surface reconstruction
STM
DFT
Photoemission spectroscopy

ABSTRACT

The Pd cyclometallated complex [(5-bromo-2-phenylpyridine)Pd(μ-Cl)]$_2$ is deposited on Ag(1 1 0) at room temperature by sublimation in ultra-high vacuum. The thermal evolution of the system is followed by scanning tunnelling microscopy and X-ray photoemission spectroscopy, while the initial and final configurations are validated by ab-initio calculations. We observe the surface induced dissociation of the molecule and the occurrence of a cross coupling reaction between the two organic fragments, leading to the surface assisted synthesis of diphenyl-bipyridine molecules. Such a process, occurring with low probability at RT, is thermally activated and competes with desorption. At variance with most cross-coupling reactions at surfaces reported in literature, in this case the reactants come from the dissociation of the same compound so that only one precursor is employed, leading to a simplified preparation protocol. The Br and Cl atoms dissociated from the molecule bind to the surface and promote an extended surface reconstruction upon annealing, which was not observed previously upon deposition of halogenated aromatic compounds.

1. Introduction

In synthetic organic chemistry, cross-coupling reactions catalyzed by a metal atom are of strategic importance since they lead to the formation of new C—C bonds. Hence, they allow to produce complex molecular architectures, possibly doped with heteroatoms, but they are also the most widespread method to synthesize several key precursors for the production of pharmaceuticals and organic compounds, such as arylalkynes and conjugated enynes. [1].

When they take place on solid surfaces, cross coupling reactions involve adjacent molecules of the same or of different species [2–4]. With respect to the reaction in solution, the process can lead to different reaction steps, and possibly to different reaction products, due to 2D confinement and to the active role of the substrate.

Among the different ways to grow 1D and 2D molecular architectures, the self-assembly and possible polymerization of properly designed precursors guarantees the best uniformity and degree of order. [2,5] Doping of such structures with non-metallic elements (e.g., N, P, S, B) [6] or with transition metal atoms (TM) can significantly affect the catalytic activity of these new materials and make them valuable candidates to replace currently used catalysts based on precious transition metals. Polymerization occurs via C—C coupling, with or without the formation of organometallic intermediates involving substrate atoms. In a common situation, the reactants present a C-halogen bond, which breaks at the metal surface. The unsaturated C atom can form either an organometallic intermediate with a metal atom of the surface (Ullmann

* Corresponding authors.
E-mail addresses: cristiana.divalentin@unimib.it (C. Di Valentin), letizia.savio@imem.cnr.it (L. Savio).
[1] These authors contributed equally.

Accepted 12 October 2022

coupling) or directly a new C—C bond with another dissociated precursor molecule, while the dissociated halogen atom binds to the surface.

Most of the attention was devoted, so far, to the organic fragments, which undergo C—C coupling to form new molecular species/nanostructures. However, halogen atoms are definitely not a spectator but have been proved to interact strongly with the surface and to influence the morphology of the final reaction products [4]. E.g., Dettmann et al. compared the thermal evolution of differently halogenate *para*-phenylenes and demonstrated that the halogen species influences the orientation of the organometallic assembly and affects the activation barriers. In particular, they observed topotactic polymerization of diiodobenzene on Cu(1 1 0) with iodine atoms sitting in rows parallel to the organometallic chains [7], while in the parallel experiment performed with bromo-iodobenzene precursors the Br atoms remain involved in the assembly and I segregates in c(2 × 2) reconstructed areas [4].

Indeed, the interaction of halogens with metal surfaces was proved to be strong and often to induce changes in the electronic structure, atomic arrangement and reactivity of the surface, with important drawbacks in heterogeneous catalysis [8,9]. E.g., missing row and c(2 × 2) reconstructions were observed upon Cl adsorption on Cu(1 1 0) [10], while LEED patterns corresponding to p(2 × 1) and c(4 × 2) overlayers were detected after Br_2 dissociation on Ag(1 1 0) [11]. On the other hand, it is well known that the addition of a small amount of chlorine to Ag catalyst drastically improves its selectivity towards ethylene epoxidation [8].

In the case of halogenated complexes at metal surfaces, the halogen atoms released in the dissociation process coexist with a high density of organic fragments and only seldom induce surface reconstruction [4]. They usually desorb in the form of hydrogen halide, provided that some H is made available by further dehydrogenation of the aromatic compounds [12] or even by exposure of the surface to atomic H [13]. In absence of available hydrogen, on the contrary, experimental evidence suggests that they desorb as diatomic molecules or metal halides or, in case of the small Cl atom, diffuse into the substrate [9,11,14].

We have recently investigated [15] the deposition of Pd cyclometallated compound [(5-bromo-2-phenylpyridine)Pd(μ-Cl)]$_2$ (CyPd in the following – see Fig. 1a for the molecular structure) on Ag(1 1 0) at RT. This complex contains two Pd atoms, stabilized in the molecular structure by formation of *N*-Pd-C bonds. We demonstrated that the molecule undergoes dissociation due to the strong interaction with the substrate. Indeed the molecule fully dehalogenate and both the Phe-Pyr fragment and the Br and Cl atoms bind to the surface. The released Pd atoms, on the contrary, diffuse into the bulk and are no longer detected. In this paper we prosecute the study of the CyPd/Ag(1 1 0) system at RT. Indeed, we report on the surface assisted synthesis of diphenylbipyridine molecules by cross coupling reaction of the phenyl-pyridine (Phe-Pyr) fragments originating from the dissociation of one single organometallic complex. Such a process, occurring with low probability at RT, is thermally activated and competes with desorption. At variance with most cross-coupling reactions at surfaces reported in literature, in this case the reactants come from the dissociation of the same molecule so that only one precursor is employed, leading to a simplified preparation protocol. The Br and Cl atoms deriving from CyPd dissociation bind at the surface and promote an extended surface reconstruction upon annealing, confirming their relevant role in the formation of C-based systems from halogenated precursors.

2. Experimental and computational methods

2.1. Synthesis

CyPd (molecular structure reported in Fig. 1a) was synthesized according to the procedure of Yian Shi et al. [16]: $PdCl_2$ was reacted with a slight excess (1:1.05) of 5-bromo-2-phenylpyridine in $CHCl_3$, at a temperature of 100 °C (sealed tube, inert atmosphere) for 24 h. The precipitate was filtered and washed several times with $CHCl_3$ to obtain pure CyPd in form of a highly insoluble yellow powder. Synthesis details and characterization of CyPd is reported elsewhere [15]. Here we mention that thermogravimetric analysis showed high thermal stability, with decomposition occurring above 320 °C. Moreover, infrared and photoemission spectra of the powders "as synthesized" and after several sublimation cycles in ultra-high vacuum (UHV) do not show remarkable differences.

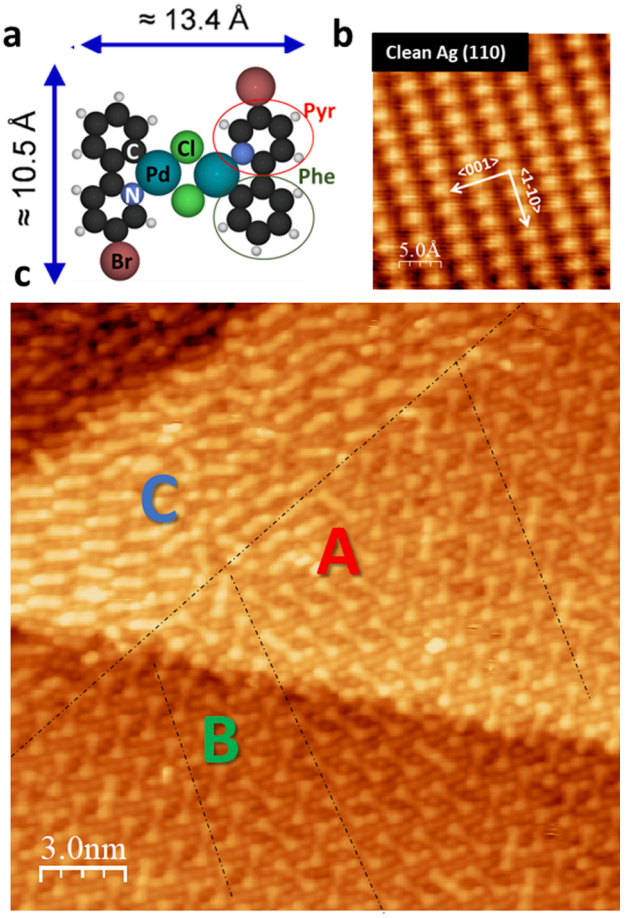

Fig. 1. a) Chemical structure of the Pd cyclometallate [(5-bromo-2-phenylpyridine)Pd(μ-Cl)]$_2$. b) Atomically resolved STM image of clean Ag(1 1 0), on which the high symmetry directions are marked (white arrows). Image size: 2.5x2.5 nm^2, V = 0.5 V, I = 0.2nA. c) STM image of the Ag(1 1 0) surface after 30 min deposition of CyPd at RT. Image size: 21x21 nm^2, V = 0.36 V, I = 0.64nA. A,B and C domains are separated by dashed lines.

2.2. Experimental methods

All experiments were performed under UHV conditions. Microscopy measurements were recorded using a Low Temperature Scanning Tunneling Microscope (LT-STM – CREATEC manufacturer) at the IMEM-DIFI laboratory in Genova, while high resolution X-ray photoemission (HR-XPS) experiments were carried out at ANCHOR-SUNDYN end-station of the ALOISA beamline at the Elettra synchrotron radiation facility (Trieste, Italy) [17].

The Ag (1 1 0) surface was cleaned by a few cycles of sputtering with Ne^+ (Ar^+) ions followed by annealing for 5 min to a temperature T = 537 °C (T = 570 °C) for microscopy (spectroscopy) experiments. The CyPd molecules were sublimated from a Ta crucible resistively heated to 130 °C and deposited on Ag(1 1 0) at room temperature (RT). The sample was eventually step-annealed for 5 min up to T = 500 °C, always keeping the background pressure lower than 2.0x10^{-9} mbar. For each annealing

step the surface morphology was monitored by STM while the chemical composition was checked by HR-XPS.

The LT-STM setup consists of the main STM chamber and of a preparation chamber; the latter is equipped with a homemade evaporator for deposition of organic molecules and with all typical vacuum facilities for sample cleaning and residual gas analysis. STM images were recorded at liquid nitrogen temperature (LN_2, 77 K) using a Pt/Ir tip. They were acquired in constant current mode, with typical tunneling currents $0.2nA \leq i \leq 0.6nA$ and bias voltage applied to the sample $-3.5\ V \leq V \leq +3.8\ V$. Surface orientation and image size were determined from atomically resolved images of clean Ag(1 1 0) (see Fig. 1b) and heights were calibrated on monoatomic Ag steps. STM analysis was performed with WSxM software [18].

High resolution photoemission experiments were carried out using a Phoibos 150 analyzer (SPECS manufacturer). XPS spectra were recorded at normal emission and at a photon energy $h\nu = 515$ eV. The instrumental resolution of 0.15 eV and the calibration of the binding energy (E_b) were determined by recording the Fermi edge of the Ag(1 1 0) substrate. After calibration, the Ag $3d_{5/2}$ line of the clean surface is found at $E_b(Ag\ 3d_{5/2}) = 368.21$ eV, in perfect agreement with literature data [19]. Core level spectra were fitted with Doniach-Sunjic line shapes convoluted with a Gaussian profile after subtraction of a linear background. An error of ± 5 % is estimated for the fitted intensities. Up to four components were necessary to reproduce the C 1 s region, while only two were sufficient for the N 1 s peak. Ag 3d, Cl 2p and Br 3d regions were fitted with doublets considering the spin–orbit splitting.

2.3. Computational methods

Density Functional Theory (DFT) calculations were performed using the plane-wave-based Quantum ESPRESSO package (QE) [20–22]. The ultrasoft pseudopotentials [23] were adopted to describe the electron–ion interaction with Ag (4d, 5 s), C (2 s, 2p), N (2 s, 2p), and H (1 s), treated as valence electrons. Energy cutoffs of 45 Ry and 360 Ry (for kinetic energy and charge density expansion, respectively) were adopted for all calculations. The Van der Waals density functional vdW-DF2^{C09x} [24], which was successfully applied to describe self-assembly of brominated tetracene and corannulene on different metal surfaces [25–28], was used for electron exchange correlation.

For the simulation of the Ag(1 1 0)-c(2 × 2) supported CyPd (CyPd/Ag-c(2 × 2)), a (6 **a** × $3\sqrt{2}$ **a**) supercell was used, where **a** is the cubic lattice parameter of Ag bulk (4.07 Å, in agreement with the experimental value). The Ag(1 1 0) surface was modeled by a three-layer slab with the bottom layer fixed to the bulk positions during the geometry relaxation to mimic a semi-infinite solid. The c(2 × 2) reconstruction was modeled by adding 0.5 ML of Ag adatoms on 4-fold hollow sites. To avoid interactions between adjacent periodic images, a vacuum space of about 18 Å in the direction perpendicular to the surface was used. The geometry relaxation of all considered systems was performed with a 2 × 3 × 1 Monkhorst- Pack k-points mesh [29].

STM simulations were performed using the Tersoff-Hamann approach [30], according to which the tunneling current is proportional to the energy-integrated Local Density of States (ILDOS). Constant current and bias voltage values in STM simulations were chosen to match the experimental values. STM images were rendered with Gwyddion software [31].

The Climbing Image − Nudged Elastic Band (CI − NEB) method [32] was employed to simulate the cross coupling process at the Ag(1 1 0)-c(2 × 2) surface, generating the minimum energy path of the reaction step and an evaluation of the energy barrier.

3. Results and discussion

3.1. RT deposition and thermal evolution

The STM image in Fig. 1c shows an overview of the Ag(1 1 0) surface after deposition of CyPd at RT for 30 min. It is evident that the adsorbate completely covers the surface. Neither bare Ag patches nor double-layer formation were observed upon careful inspection of several sample areas, therefore we can safely conclude that full monolayer coverage has been reached and that the process is self-limiting. In our previous publication [15] we demonstrated that CyPd molecules self-assemble on Ag (1 1 0) at RT also at sub-monolayer coverage, but we found a self-assembled pattern different from those reported in the following. We mention that the experimental conditions (sample temperature, CyPd sublimation temperature and deposition time) were nominally the same in both experiments, but no full monolayer coverage could be reached in the previous work. We deduce that the molecular flux on the surface was significantly lower and, indeed, XPS experiments indicate that this parameter generally increases after several sublimation cycles, i.e. when the molecules get better outgassed. Therefore, we suggest that the kinetics of the self-assembly process plays a role in determining the final structure. If the flux is low, the molecules land on the surface and have time to dissociate, diffuse and interact with Ag atoms. Increasing the flux, the mobility of molecules/fragments is reduced and the probability of inter-molecular interactions during the formation of the self-assembly gets larger and may lead to completely different arrangement, as discussed in the following.

Three different self-assembled geometries (labelled A, B and C in the following) coexist in Fig. 1c. Fig. S1 in the Supporting Material (SM) shows separate surface areas covered by extended domains of each of these structures. The common feature among them is the presence of stick-shaped units separated by dots and oriented ±30° off the <1 −1 0> direction, which acts then as a mirror axis. In domain A, all the sticks have the same orientation, while in domain B adjacent sticks have opposite orientation and form a sort of zig-zag pattern (see also enlarged images in Fig. 3 and Fig. S1b). Since it is difficult to distinguish A and B domains of the smallest size, for simplicity and to be able to define a unit cell we identify a domain as of A or B type if it contains a minimum of four sticks with the same or with alternating orientation, respectively. In structure C, the same sticks observed in structures A and B appear as minority structures, being surrounded by shorter features with a brighter end. Also a few diamond-shaped features are randomly present (see top-right corner of domain C in Fig. 1c). Arrangement C has a short-range and much lower degree of order and it disappears above RT. The presence of less ordered assemblies, which do not correspond to the minimum of energy, is reasonable when the flux is sufficiently high [33]. However, structure C will not be discussed in further details.

After deposition at RT, the sample was step annealed up to a maximum temperature T = 450 °C to investigate the thermal evolution of the self-assembled layers. Annealing to 100 °C causes the disappearance of assembly C, a reduction in the extension of B and an increase of the area covered by assembly A. Such behavior suggests that the most ordered geometry is also the most stable one. We anticipate that, at this T, two new structures appear (see Fig. 5): the former (labelled I) consists of isolated sticks lying on a c(2x2) reconstructed surface; it becomes dominant at 200 °C and is almost completely removed at 250 °C. The latter (R) consists of bare Ag(1 1 0) areas with a (2x1) reconstruction. The area covered by structure R increases from 100 °C to 350 °C, at which T it extends almost over the whole surface. Above 450 °C, the reconstruction is lifted and clean, unreconstructed Ag(1 1 0) terraces appear in STM images.

For a better identification of the observed structures, deposition and thermal evolution of the CyPd/Ag(1 1 0) system was investigated in parallel by HR-XPS. Fig. 2 reports XPS spectra of the N 1 s, C 1 s, Cl 2p and Br 3d regions for saturation coverage at RT, i.e. for a full monolayer of CyPd on Ag(1 1 0) according to STM data, and upon step annealing to 500 °C.

At RT, doublets are present at 68.1 and 69.1 eV and at 197.6 and 199.2 eV in the Br 3d and Cl 2p regions, respectively. The absence of a Br-C component at $E_b(Br\ 3d_{5/2}) \sim 70.4$ eV indicates that the molecule is fully debrominated and the Br atoms are bound to Ag. Unfortunately, it

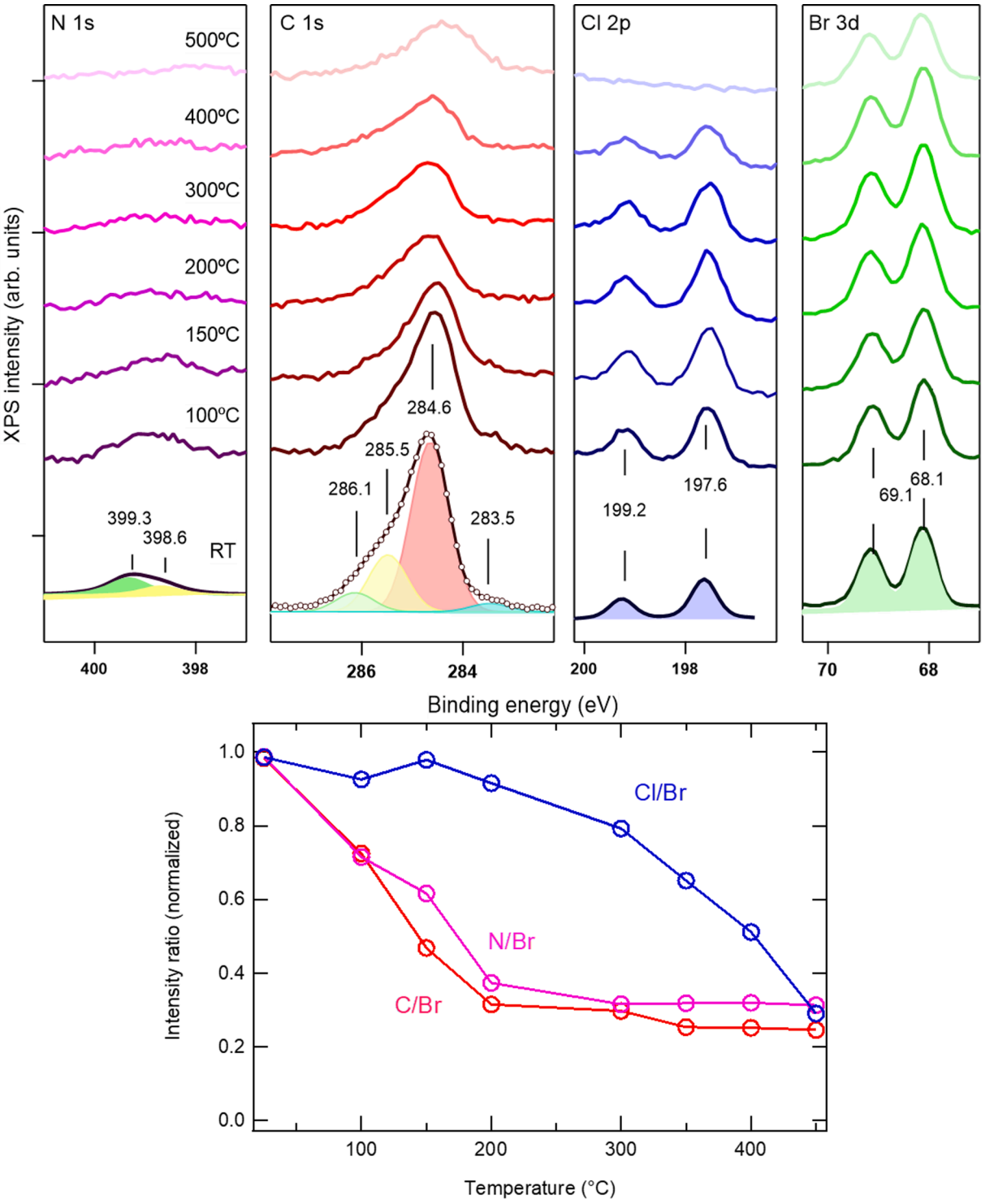

Fig. 2. Top: Photoemission core level spectra of N 1 s (purple), C 1 s (red), Cl 2p (blue) and Br 3d (green) lines for the CyPd/Ag(1 1 0) system obtained upon 24 min of deposition at RT and following step-annealing up to 500 °C. Traces are normalized to the background of the corresponding spectrum recorded for clean Ag(1 1 0) (not shown) and upshifted for sake of clarity. hν = 515 eV, pass energy = 25 eV. Bottom: Thermal behavior of the C 1 s, N 1 s and Cl 2p lines. For a better visualization and to avoid systematic errors, the total C 1 s, N 1 s and Cl 2p areas are normalized to the corresponding Br 3d signal (assumed as constant) and to the value at RT. (For interpretation of the references to color in this figure legend, the reader is referred to the web version of this article.)

is not possible to determine if Cl atoms are still bound to the molecule, since the expected binding energy for Cl-Pd and for Cl-Ag bonds are very close [34].

C 1 s and N 1 s spectra appear as broad asymmetric peaks with maxima at 284.6 eV and 399.3 eV respectively. In accordance with previous analysis [15], we fit the C 1 s line with four peaks at 283.5 eV, 284.6 eV, 285.5 eV and 286.1 eV, respectively. The low E_b peak is attributed to C-Ag bonds, which form after molecule dissociation; the one at 284.7 eV is ascribed to the convolution of C atoms involved in C—C and C—H bonds while the other two components are related to C—N with the pyridine ring in different configurations with respect to the substrate [35]. Correspondingly, the N 1 s line is fitted with two

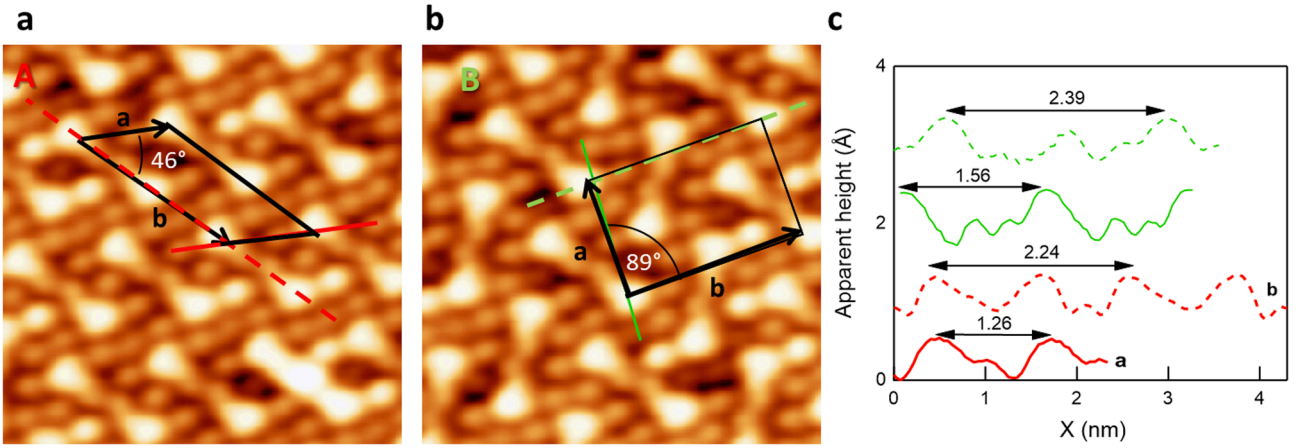

Fig. 3. a) and b): Close-up STM images (5 × 5 nm^2) of the overview in Fig. 1, showing the details of structures A and B, respectively. The unit cells are marked in black. , for structure A and , for structure B, being the primitive unit vectors of Ag(1 1 0) in the ⟨0 0 1⟩ and <1 −1 0 > directions, respectively. c) Height profiles cut along the paths marked in panels a) and b) and corresponding to the unit cell sides.

components at 398.6 eV and 399.3 eV. Both species are suitable for N atoms in the pyridinic ring but have a slightly different interaction with the Ag substrate [35] The high energy component is similar to the one observed for bi-isonicotinic acid on Ag(1 1 1) and identified with nitrogen atoms weakly interacting with the substrate [36]. Viceversa, the 398.6 eV line is compatible with the signal measured for *N*-doped graphene on Ni(1 1 1) [37] and, as already suggested in ref. [15], it could be indicative of a stronger interaction with the surface and possibly of the formation of *N*-Ag bonds.

The Pd 3d region is not reported since it shows no Pd related features; as discussed in ref. [15], this is indicative that Pd diffuses into the bulk and does not contribute to the XPS spectra.

As evident from the spectral sequence of Fig. 2, changes in the C 1 s and N 1 s intensity occur from the first annealing steps, while the Cl and Br signals remain stable till 300 °C and 450 °C (spectrum not shown), respectively. Therefore, to better visualize the thermal evolution of the layer, we take the Br 3d signal as a reference and we plot the C/Br, N/Br and Cl/Br area ratio in the bottom panel of Fig. 2. Since we are interested in comparing the trend of the different elemental constituents of CyPd and not in their absolute values, all the traces are further normalized to the value at RT. The graph shows that C and N present the same behavior: their intensity reduces to less than 40 % of the original value when annealing from RT to 200 °C, indicating partial desorption of the organic part of the CyPd molecule. Then the peak areas remain almost stable while the peaks broaden and downshift in binding energy. We associate the residual C 1 s and N 1 s intensity to a degradation of the remaining Phe-Pyr units; most probably the phenyl and/or pyridine rings break and smaller fragments bind to the Ag surface. On the contrary, the Cl and Br intensity is stable to much higher temperatures: Br remains on the surface over the full annealing range, while the Cl intensity drops above 300 °C. Considering the small dimensions of Cl and the higher desorption temperatures reported in literature [14], we suggest that some diffusion into the bulk may be responsible of the initial reduction of intensity. The overall higher thermal stability of halogen species indicates that the interaction with the substrate is stronger for the halogen atoms than for the organic fragments.

Finally, we mention that: i) at RT, C:Br, C:Cl and C:N ratios are close to the stoichiometric value of 11:1, though actually slightly deficient in C [15]; ii) the XPS spectra are perfectly compatible to those reported in ref. [15], showing the absence of Pd at the surface, the dissociation of Br and the different thermal stability of halogen atoms and of the Phe-Pyr fragments. Such behavior strongly suggests that the chemistry at the surface is the same and that also in the present case the molecules dissociate upon deposition on the surface.

3.2. *Extended assemblies of type A and B*

Fig. 3 shows an enlargement of self-assemblies A and B, in which their geometry appears in better detail. The unit cell of structure A is defined by a black rhomboid with sides a=(1.26 ± 0.01) nm and b=(2.24 ± 0.04) nm. These vectors are oriented −12° and −58° off the ⟨0 0 1⟩ direction, respectively, and form an angle α=(46 ± 3)° with each other. The unit cell contains one stick oriented nearly parallel to the **b** vector, and 6 dots of different brightness. Comparing the experimentally determined periodicities with the size of a CyPd molecule (1.34 nm long and 1.05 nm wide), we estimate a population of one molecule per unit cell, corresponding to a local coverage of (4.9 ± 0.1)·10^{13} molecules/cm^2. For structure B, the unit cell is nearly rectangular, with a=(1.56 ± 0.02) nm, b=(2.39 ± 0.06) nm, α=(89 ± 3)°, and with vector **b** parallel to the ⟨0 0 1⟩ direction. The unit cell contains 2 sticks, oriented at + 30° and −30° off <1 −1 0>, respectively, and 8 interstitial dots. Therefore, in this case the assembly is slightly more compact, accommodating (5.3 ± 0.1)·10^{13} molecules/cm^2. For both structures A and B, the unit cell parameters measured at RT and after annealing are compatible within the error.

The sticks are the basic constituents of the assemblies and they are present in two different shapes: in most cases they have a minimum at the center, but a few sticks with a central maximum appear in each overview. The high resolution STM image of Fig. 4ab and the corresponding line scans of Fig. 4c emphasize this difference, also taking advantage of the use of different color contrasts (panels a and b). Sticks showing a minimum at their center (green continuous trace in panel c) are formed by two “comma-like” features facing each other. Each of them consists of a bright lobe (L) at the end of the stick and of a smaller and fainter lobe (F) pointing towards its center but misaligned with respect to the stick axis. Sticks with a maximum at their center present, on the contrary, a central lobe (L_c) slightly more protruding than the lateral ones (green dashed trace in panel c). The overall length is ~ 1.7 nm for both structures. The relative population of bright sticks in the compact assemblies of type A and B varies from 10 % to 20 % depending on T, as indicated in the histogram in panel d. Sticks are surrounded by several dots of alternating brightness. Since their density exceeds the number of halogen atoms expected for each molecule, we infer that they correspond both to halogen and Ag atoms and indicate that a significant reorganization of surface atoms occurs upon CyPd adsorption and dissociation.

3.3. *Isolated structure and surface reconstruction*

According to XPS inspection, after annealing the sample to 100 °C,

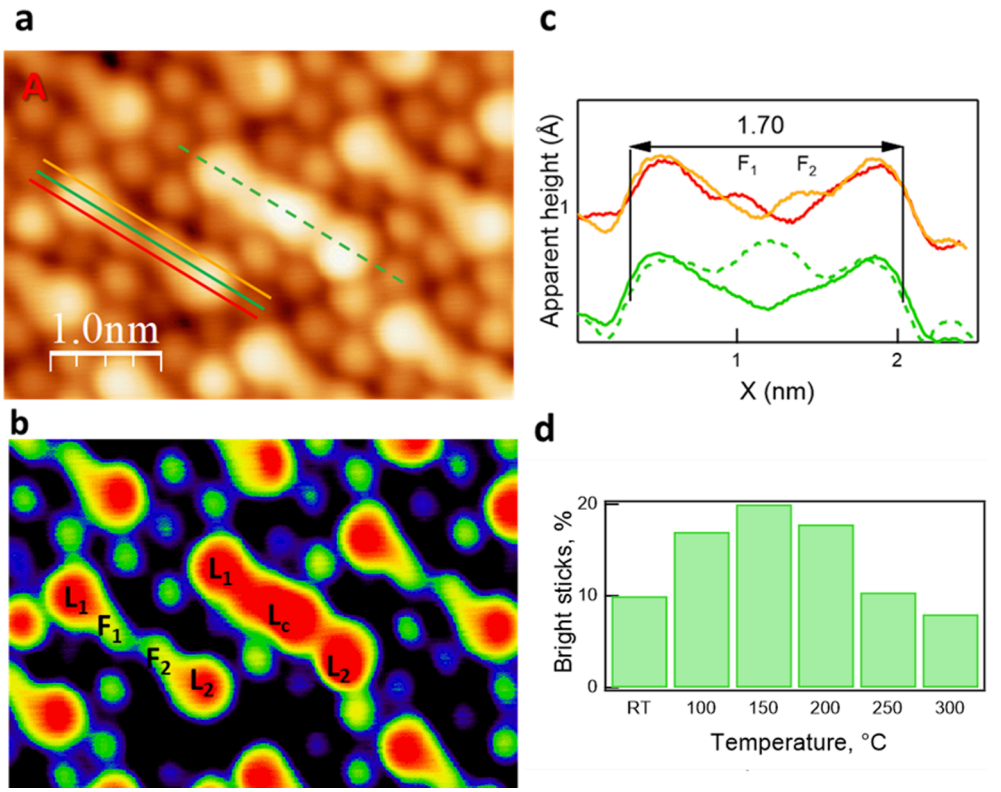

Fig. 4. a) High resolution STM image of structure A recorded after annealing the sample to 150 °C for 5 min (4.5 × 3.1 nm^2, V = -0.1 V, i = 0.2nA). b) Same image of panel a) plotted with a different color palette to better highlight details. c) Height profiles cut along the traces marked in panel a. d) Histogram showing the distribution of bright sticks in domains A and B.

desorption of the Phe-Pyr units occurs. Coherently, sample areas with little or no molecule-related features appear in STM images. Fig. 5a shows a STM overview of the Ag(1 1 0) surface after annealing to 200 °C. Most of the surface is covered by structure I, which consists of isolated sticks oriented ± 60° off the <1 −1 0> direction. They sit on top of Ag terraces presenting a slightly compressed hexagonal pattern (see panel b). For fcc crystals, such pattern corresponds to a c(2x2) reconstruction of the (1 1 0) face. In addition, a few areas with a rectangular pattern

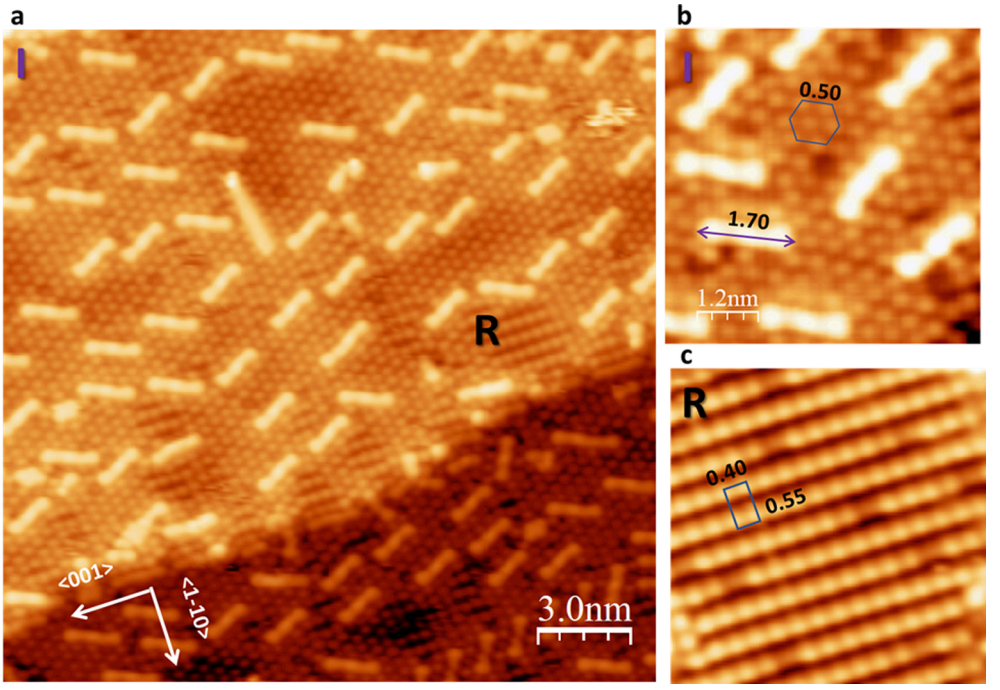

Fig. 5. a): Overview STM image of the Ag(1 1 0) surface covered with structure I. Domains with reconstructed p(2 × 1) surface are also present and labelled as R. The image was recorded after step-annealing the sample to 200 °C for 5 min (20 × 20 nm^2, V = 0.5 V, i = 0.2nA). b) and c): Close-ups of I and R structures (6 × 6 nm^2, V = -0.5 V). The unit cell of the reconstructed surface is reported on both panels; dimensions are expressed in nm.

typical of a p(2x1) reconstruction of the substrate (indicated by R – see unit cell dimensions and orientation marked in panel c) are visible in the overview. Such patches grow with T and cover most of the surface at 350 °C. We remark that no molecular features are found on the R structure, indicating that it becomes energetically favored only after complete local desorption of the organic fragments.

All the sticks in I present a central bright lobe and are ~ 1.7 nm long, thus, they highly resemble those already discussed for assemblies A and B. The different orientation (±60° off <1 −1 0> instead of ± 30° for the compact structures) could be related to the low density and/or to the symmetry of the reconstructed Ag terrace. To determine the atomic structure and conformation of these bright sticks, we performed a DFT study starting from a model consistent with the experimental evidence. We recall that XPS data suggests dissociative adsorption of CyPd on Ag (1 1 0), followed by Pd atoms diffusion into the substrate, while Cl and Br atoms disappear only for T > 300 °C and T > 450 °C, respectively. Based on this information, we assume that each stick is formed by two Phe-Pyr units (as defined in Fig. 1a) anchored to the Ag surface. Halogen atoms are not explicitly present in the model, because we consider that they bind to a surface Ag atom immediately after dissociation from the organic fragments, and act then as spectators. Similarly, Pd atoms are not explicitly considered in the proposed model since, based on our previous calculations [15], they are expected to become buried beneath the Ag surface.

The proposed adsorption models for dissociated CyPd on the Ag (1 1 0)-c(2x2) surface are reported in Fig. 6, starting from two Phe-Pyr units in a *trans* configuration (see Fig. 6a). The *trans* configuration, in which N atoms of the Pyr rings are on opposite sides of the two units (see blue atoms in the red box of Fig. 6a), is expected to form after dissociation of a CyPd molecule and diffusion of the fragments on the surface. The optimized dimeric organometallic structure, named *trans* (Phe-Pyr)$_2$Ag, presents the two Phe-Pyr units almost aligned to each other and linked together through one Ag adatom (1), thus forming two bridging organometallic C-Ag-C bonds. Each Phe-Pyr unit is also anchored to another Ag adatom (2) by C-Ag and *N*-Ag bonds. It is worth noting that this configuration is stabilized through the passivation of all dangling bonds (produced by dissociation of the Pd and halogen atoms from the original molecule) by the Ag substrate, and that the new C-Ag and *N*-Ag bonds are responsible for the molecule orientation. The optimized model does not display any geometrical atomic protrusion at the expected location for the Ag adatom (as shown from the side view in Fig. 6a), and it is thus consistent with the experimentally observed sticks with central minimum (Fig. 4a and b) observed in structures A and B. Indeed, the corresponding simulated STM image (see Fig. 7a) well reproduces the experimental image of the repeating unit of arrangements A and B (Figs. 3 and 4), showing two features with brighter lobes towards the outside and fainter lobes facing each other.

To explain why sticks in structure I (and in smaller numbers also in structures A and B) present a bright central lobe, we considered the possibility that a C—C coupling reaction occurs, which converts (Phe-Pyr)$_2$Ag into the organic dimer 6,6′-diphenyl-3,3′-bipyridine (Phe-Pyr)$_2$. Direct conversion from *trans* (Phe-Pyr)$_2$Ag (in Fig. 6a) to *trans* (Phe-Pyr)$_2$ (Fig. 6c), although largely exothermic (-2.12 eV), is likely to be kinetically hindered. In fact, the formation of the new C—C bond requires the

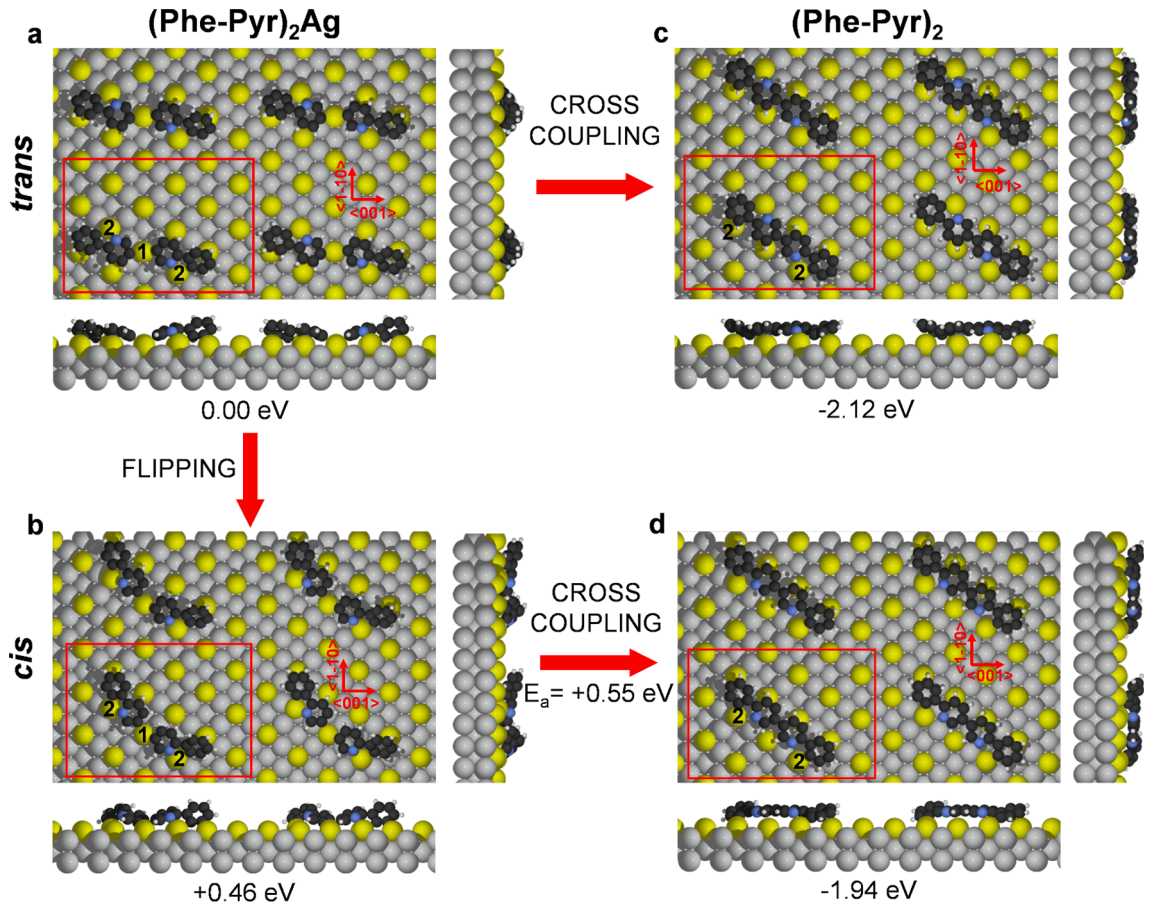

Fig. 6. Top and side views for adsorption models of CyPd on Ag(1 1 0)-c(2 × 2). The two main crystallographic directions (⟨0 0 1⟩ and <1 −1 0>) are indicated by the red arrows. The (6 × 3$\sqrt{2}$) supercell is shown in red. Relative energies (with respect to configuration **a**) are reported below each panel (in eV). Color coding: Ag atoms belonging to Ag(1 1 0) surface are in gray, Ag adatoms due to the c(2 × 2) reconstruction are in yellow, C atoms are in black, N atoms are in blue, and H atoms are in white. Ag adatoms interacting with the molecular fragments are labeled as (1) and (2), as described in the text. (For interpretation of the references to color in this figure legend, the reader is referred to the web version of this article.)

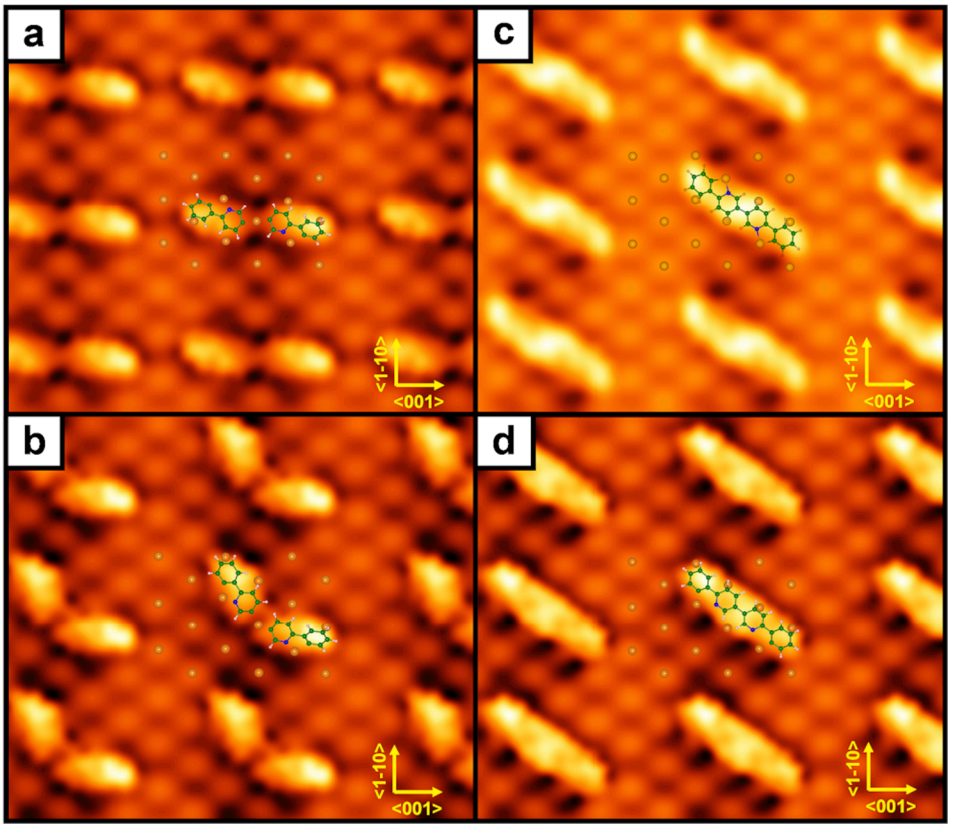

Fig. 7. Simulated STM images of the models reported in Fig. 6. Panels a, b, c, and d correspond to geometries a, b, c, and d of Fig. 6, respectively. Yellow lines indicate the two main crystallographic directions: ⟨001⟩, and <1 −1 0>. Atoms of the CyPd molecule (C in green, N in blue, and H in white) and the Ag adatoms (in orange) contained in the ($6 \times 3\sqrt{2}$) supercell are superimposed on the image to facilitate its understanding. V = − 0.1 V, ILDOS isosurface value of 5×10^{-5} $|e|/a_0^3$. (For interpretation of the references to color in this figure legend, the reader is referred to the web version of this article.)

two Phe-Pyr fragments to move over the surface and around the Ag adatom (1) till they get close enough for the C—C coupling. These adjustments could be energetically demanding since one organic fragment (e.g. the one on the left) must break a strong interaction with the Ag adatom (2) on the same row of Ag adatom (1) and establish a new bond with a Ag adatom in another row (compare Fig. 6a and 6c). Therefore, we propose the alternative easier path shown in Fig. 6bd: one Phe-Pyr unit of *trans* $(Phe\text{-}Pyr)_2Ag$ flips on the surface around the Ag adatom (2), without need to detach from both Ag adatom (1) and (2), and converts into the *cis* $(Phe\text{-}Pyr)_2Ag$ conformer (Fig. 6b). Starting from this new conformer, the C—C coupling can take place more easily and lead directly to the final *cis* $(Phe\text{-}Pyr)_2$ product (in Fig. 6d). In this case, no detachment of the Phe-Pyr unit from the surface is needed because the two C atoms are now on the same side of the Ag(2)-Ag(1)-Ag(2) row. The activation barrier for this last step is computed to be 0.55 eV. Note that the simulated STM image of *cis* $(Phe\text{-}Pyr)_2$ (in Fig. 7d) is in better agreement with the experimental images of sticks with a central maximum (in Fig. 5b) than the corresponding simulated STM image of *trans* $(Phe\text{-}Pyr)_2$ (in Fig. 7c). Simulated STM images for all models reported in Fig. 6 at different bias voltages (+/- 0.1 V and +/- 0.5 V) are shown in the SI (see Figs. S2 to S5). Experimentally, we observe that the density of bright sticks increases after the first annealing steps (see Fig. S6 in SI), though the overall molecular coverage at the surface decreases significantly. This evidence is coherent with the small activation barrier found by DFT calculations in the conversion from configuration a) to d) (in Fig. 6) and confirms that this mechanism competes with desorption.

To summarize, from the DFT investigation above, the following picture emerges: the CyPd molecules land on the surface and dissociate; the two newly formed Phe-Pyr fragments align along a Ag(2)-Ag(1)-Ag(2) row; the dangling N and C bonds saturate towards the same Ag adatom (2), while the dangling C bond resulting from debromination saturates towards another Ag adatom (1) of the same row, forming a *trans* $(Phe\text{-}Pyr)_2Ag$ species (Fig. 6a). The overall appearance in STM images is a stick-shaped structure with a minimum at the center (in line with Figs. 3 and 4). When enough energy is provided by annealing to at least 100 °C, a fast *trans–cis* interconversion occurs (Fig. 6b), followed by C—C coupling and formation of a *cis* $(Phe\text{-}Pyr)_2$ compound (Fig. 6d). Since the latter lies flat on the surface, it appears as a stick with a central maximum (in line with structure I in Fig. 5).

Although the simulations were performed for an isolated CyPd unit, we believe that they are explicative also of the behavior of the self-assemblies A and B, in which the sticks are close-packed together. We can therefore identify the sticks with a central minimum with coupled Phe-Pyr fragments saturated towards a central Ag atom ($(Phe\text{-}Pyr)_2Ag$) and the ones with central maximum with the $(Phe\text{-}Pyr)_2$ units. As already mentioned, the different orientation of sticks in structures A and B and in structure I is most probably related to the additional interaction with the surface and neighboring molecules in the self-assembled domains. In structure I, the orientation of sticks is governed by two factors: i) the passivation of the two undercoordinated C atoms of the Phe rings through the formation of C-Ag bonds (see Ag adatoms labeled as 2 in Fig. 6c and d); ii) the planarization of the $(Phe\text{-}Pyr)_2$ product as a result of the cross-coupling reaction, which is possible since the rows of Ag adatoms are far enough not to hinder the relaxation of the molecule to a planar structure. To fulfill these two requirements, and given the symmetry of the c(2×2) reconstructed surface, the best arrangement for the sticks is in between two Ag rows (see yellow atoms in Fig. 6c and d) and oriented ∼ 60° off the <1 −1 0> direction.

Therefore, our combined experimental and theoretical analysis suggests that surface assisted synthesis of the $(Phe\text{-}Pyr)_2$ compound occurs on Ag(1 1 0) by cross-coupling reaction of the two identical organic fragments generated by dissociation of a single organometallic CyPd unit. This is at variance with the majority of cross coupling reactions, which most often are used to build larger compounds or complex molecular architectures starting from the co-adsorption of different molecular species or from different molecules of the same precursor.

Finally, we should address the role of halogens and the presence of a

surface reconstruction. We recall that Cl and Br remain stable at the surface up to temperatures much higher than the Phe-Pyr units. In particular, Br is stable well above the values measured in similar experiments leading to surface assisted synthesis of C-based networks [2,13,25]. An efficient desorption mechanism for halogen atoms chemisorbed on metals is to react with H and leave the surface in the form of hydrogen halide. E.g., this was the case for di-bromo-pyrene, di-bromo-benzene and di-bromo-tetracene [2,12,13] on Ag or Cu surfaces. In those works, H is provided by further thermal induced dehydrogenation of the precursor molecule, or even by controlled exposure of the sample to a flux of atomic H [13]. The situation is different in the present case, since no additional C—H bonds are broken upon annealing; instead, Phe-Pyr units are likely to desorb intact or to cross-couple to form $(Phe\text{-}Pyr)_2$. We believe that the unavailability of H is the reason for the higher thermal stability of halogens with respect to other literature data, since they will desorb as diatomic molecules or metal halides [9,11,14] or, in case of Cl, may diffuse into the substrate [14].

Isolated sticks sit on a c(2x2) reconstructed surface, while a p(2x1) pattern appears in areas where all the $(Phe\text{-}Pyr)_2$ units have desorbed. Coherently, the latter domains get more and more extended with increasing T, i.e., when the coverage of organic fragments reduces. This is indicative of a strong surface rearrangement upon interaction with CyPd. We mention that, due to their open structure, (1 1 0) faces of fcc crystals are prone to surface reconstruction and roughening [38]. Such reorganization is certainly favored by the strong mobility of Ag adatoms, provided by step edges [39], and by the presence of halogen atoms, which are known to form superstructures on several metal surfaces [9,11]. However, we believe the present situation to be more complex. On the one hand, some atom reorganization is evident already at RT but, due to the dense packing of organic structures, it is not possible to understand if the surface underneath the adsorbates is reconstructed or if the additional atoms simply surround the sticks. Indeed, each Phe-Pyr fragment anchors to two Ag adatoms according to our model and it is reasonable that this is a driving mechanism for the displacement of Ag adatoms. On the other hand, we believe that halogens have a role in the reconstructed phases observed above RT, but that the observed superstructure is due to Ag adatoms. We base our statement on the following observations: i) the halogen coverage (nearly 1/4 of ML at RT) is not sufficient to justify the extended reconstruction observed as due to Cl and/or Br atoms; ii) control measurements performed by depositing the parent non-brominated CyPd molecule ($C_{22}H_{16}Cl_2N_2Pd_2$ – data not shown) lead to different organic structures but to the same c(2x2) reconstruction upon annealing the sample; iii) the c(2x2) reconstruction coexists with the isolated sticks and is observed in a T range in which both Cl and Br are stable on the surface. When the Cl signal decreases significantly ($T \geq 300$ °C), only clean, p(2x1)-reconstructed terraces are observed by STM. Therefore, we suggest that halogen atoms promote surface reconstruction, as previously reported for other elements on Ag (1 1 0) [40,41]. Both halogen species are present on c(2x2) reconstructed areas while only Br atoms are likely to participate in the formation of the p(2x1) pattern.

4. Conclusions

We reported on the surface assisted synthesis of diphenyl-bipyridine molecules by cross coupling reaction originating from the deposition and dissociation of a single organometallic complex.

Indeed, a full monolayer of the Pd cyclometallate [(5-bromo-2-phenylpyridine)Pd(μ-Cl)]$_2$ was deposited on Ag(1 1 0) by sublimation in UHV conditions. Similarly to what is observed in the sub-monolayer regime [15], CyPd dissociates upon interaction with the metal surface. In our analysis we focus on what happens to the Phe-Pyr fragments which, in the present conditions, saturate towards Ag atoms forming the organometallic complex $(Phe\text{-}Pyr)_2$-Ag. Eventually, a cross coupling reaction between the two equivalent fragments originating from the precursor molecule occurs to produce $(Phe\text{-}Pyr)_2$. This process is thermally activated and competes with desorption of the organic fragments. We propose that it occurs through and intermediate step in which one Phe-Pyr unit of the organometallic complex flips into *cis*-position. The very good agreement between the simulated STM images of the initial and final configurations and the experimental ones supports the validity of our conclusions.

Finally, the Ag substrate is deeply perturbed by CyPd adsorption. Halogen atoms released by the molecules bind to the substrate and promote a reconstruction, which is c(2x2) around the isolated $(Phe\text{-}Pyr)_2$ units and p(2x1) in areas where complete desorption of the organic part has occurred. This behavior suggests an active role of halogen species in the reorganization of the surface morphology.

Associated Content.

– The supporting information file contains the following material, referenced in the text:
– Additional overviews of structures A, B and C.
– Additional STM images of the structures in Fig. 6 simulated at different bias.
– Surface density of bright sticks vs T.

Declaration of Competing Interest

The authors declare that they have no known competing financial interests or personal relationships that could have appeared to influence the work reported in this paper.

Data availability

Data will be made available on request.

Acknowledgments

We acknowledge financial support from MIUR (project PRIN2017 n. 2017NYPHN8) and from Fondazione Compagnia di S. Paolo (project MC-nano). We acknowledge Elettra Sincrotrone Trieste for providing access to its synchrotron radiation facilities and for financial support.

We thank Thuy Hien Dinh for collaboration in the initial stages of the XPS data analysis.

Appendix A. Supplementary data

Supplementary data to this article can be found online at https://doi.org/10.1016/j.apsusc.2022.155307.

References

[1] R. Chinchilla, C. Nájera, Recent advances in Sonogashira reactions, Chem. Soc. Rev. 40 (2011) 5084–5121, https://doi.org/10.1039/c1cs15071e.
[2] M. Smerieri, I. Píš, L. Ferrighi, S. Nappini, A. Lusuan, C. Di Valentin, L. Vaghi, A. Papagni, M. Cattelan, S. Agnoli, E. Magnano, F. Bondino, L. Savio, Synthesis of graphene nanoribbons with a defined mixed edge-site sequence by surface assisted polymerization of (1,6)-dibromopyrene on Ag(110), Nanoscale. 8 (2016) 17843–17853, https://doi.org/10.1039/c6nr05952j.
[3] C. Sánchez-Sánchez, F. Yubero, A.R. González-Elipe, L. Feria, J.F. Sanz, R. M. Lambert, The flexible surface revisited: Adsorbate-induced reconstruction, homocoupling, and sonogashira cross-coupling on the Au(100) surface, J. Phys. Chem. C. 118 (2014) 11677–11684, https://doi.org/10.1021/jp501321u.
[4] G. Galeotti, M. Di Giovannantonio, J. Lipton-Duffin, M. Ebrahimi, S. Tebi, A. Verdini, L. Floreano, Y. Fagot-Revurat, D.F. Perepichka, F. Rosei, G. Contini, The role of halogens in on-surface Ullmann polymerization, Faraday Discuss. 204 (2017) 453–469, https://doi.org/10.1039/c7fd00099e.
[5] J. Hu, J. Hu, Z. Zhang, K. Shen, Z. Liang, H. Zhang, Q. Tian, P. Wang, Z. Jiang, H. Huang, J.W. Wells, F. Song, Ullmann coupling of 2,7-dibromopyrene on Au(1 1 1) assisted by surface adatoms, Appl. Surf. Sci. 513 (2020), 145797, https://doi.org/10.1016/j.apsusc.2020.145797.
[6] C.N.R. Rao, K. Gopalakrishnan, A. Govindaraj, Synthesis, properties and applications of graphene doped with boron, nitrogen and other elements, Nano Today. 9 (2014) 324–343, https://doi.org/10.1016/j.nantod.2014.04.010.
[7] D. Dettmann, G. Galeotti, O. MacLean, M. Tomellini, M. Di Giovannantonio, J. Lipton-Duffin, A. Verdini, L. Floreano, Y. Fagot-Revurat, D.F. Perepichka,

F. Rosei, G. Contini, Identification of Topotactic Surface-Confined Ullmann-Polymerization, Small. 17 (2021) 1–10, https://doi.org/10.1002/smll.202103044.
[8] J.G. Serafin, A.C. Liu, S.R. Seyedmonir, Surface science and the silver-catalyzed epoxidation of ethylene: An industrial perspective, J. Mol. Catal. A Chem. 131 (1998) 157–168, https://doi.org/10.1016/S1381-1169(97)00263-X.
[9] B.V. Andryushechkin, T.V. Pavlova, K.N. Eltsov, Adsorption of halogens on metal surfaces, Surf. Sci. Rep. 73 (2018) 83–115, https://doi.org/10.1016/j.surfrep.2018.03.001.
[10] B.V. Andryushechkin, V.V. Cherkez, T.V. Pavlova, G.M. Zhidomirov, K.N. Eltsov, Structural transformations of Cu(110) surface induced by adsorption of molecular chlorine, Surf. Sci. 608 (2013) 135–145, https://doi.org/10.1016/j.susc.2012.10.005.
[11] C. Benndorf, B. Krüger, Adsorption and reaction of bromine with Ag(110), Surf. Sci. 151 (1) (1985) 271–288, https://doi.org/10.1016/0039-6028(85)90466-2.
[12] C. Bronner, J. Björk, P. Tegeder, Tracking and removing br during the on-surface synthesis of a graphene nanoribbon, J. Phys. Chem. C. 119 (2015) 486–493, https://doi.org/10.1021/jp5106218.
[13] M. Abyazisani, J.M. MacLeod, J. Lipton-Duffin, Cleaning up after the Party: Removing the Byproducts of On-Surface Ullmann Coupling, ACS Nano. 13 (2019) 9270–9278, https://doi.org/10.1021/acsnano.9b03812.
[14] M. Bowker, K.C. Waugh, Chlorine adsorption and chloridation of Ag(110), Surf. Sci. 155 (1985) 1–14, https://doi.org/10.1016/0039-6028(85)90399-1.
[15] M. Stojkovska, D. Perilli, J.E. Barcelon, M. Smerieri, G. Carraro, T.H. Dinh, L. Vattuone, M.A. Rocca, G. Bracco, M. Dell'Angela, R. Costantini, A. Cossaro, L. Vaghi, A. Papagni, C. Di Valentin, L. Savio, Well-Ordered Surface Metal Atoms Complexation by Deposition of Pd Cyclometallated Compounds on Ag (110), Appl. Surf. Sci. 606 (2022), 154960, https://doi.org/10.2139/ssrn.4158267.
[16] X. Peng, Y. Zhu, T.A. Ramirez, B. Zhao, Y. Shi, New reactivity of oxaziridine: Pd(II)-catalyzed aromatic C-H ethoxycarbonylation via C-C bond cleavage, Org. Lett. 13 (2011) 5244–5247, https://doi.org/10.1021/ol2021252.
[17] R. Costantini, M. Stredansky, D. Cvetko, G. Kladnik, A. Verdini, P. Sigalotti, F. Cilento, F. Salvador, A. De Luisa, D. Benedetti, L. Floreano, A. Morgante, A. Cossaro, M. Dell'Angela, ANCHOR-SUNDYN: A novel endstation for time resolved spectroscopy at the ALOISA beamline, J. Electron Spectros. Relat. Phenomena. 229 (2018) 7–12, https://doi.org/10.1016/j.elspec.2018.09.005.
[18] I. Horcas, R. Fernández, J.M. Gómez-Rodríguez, J. Colchero, J. Gómez-Herrero, A. M. Baro, WSXM: A software for scanning probe microscopy and a tool for nanotechnology, Rev. Sci. Instrum. 78 (2007), 013705, https://doi.org/10.1063/1.2432410.
[19] P.H. Citrin, G.K. Wertheim, Y. Baer, Surface-atom x-ray photoemission from clean metals: Cu, Ag, and Au, Phys. Rev. B. 27 (1983) 3160–3175, https://doi.org/10.1103/PhysRevB.27.3160.
[20] P. Giannozzi, S. Baroni, N. Bonini, M. Calandra, R. Car, C. Cavazzoni, D. Ceresoli, G.L. Chiarotti, M. Cococcioni, I. Dabo, A. Dal Corso, S. de Gironcoli, S. Fabris, G. Fratesi, R. Gebauer, U. Gerstmann, C. Gougoussis, A. Kokalj, M. Lazzeri, L. Martin-Samos, N. Marzari, F. Mauri, R. Mazzarello, S. Paolini, A. Pasquarello, L. Paulatto, C. Sbraccia, S. Scandolo, G. Sclauzero, A.P. Seitsonen, A. Smogunov, P. Umari, R.M. Wentzcovitch, QUANTUM ESPRESSO: A modular and open-source software project for quantum simulations of materials, J. Phys. Condens. Matter. 21 (39) (2009) 395502.
[21] P. Giannozzi, O. Baseggio, P. Bonfà, D. Brunato, R. Car, I. Carnimeo, C. Cavazzoni, S. De Gironcoli, P. Delugas, F. Ferrari Ruffino, A. Ferretti, N. Marzari, I. Timrov, A. Urru, S. Baroni, Quantum ESPRESSO toward the exascale, J. Chem. Phys. 152 (2020), 154105, https://doi.org/10.1063/5.0005082.
[22] P. Giannozzi, O. Andreussi, T. Brumme, O. Bunau, M.B. Nardelli, M. Calandra, R. Car, C. Cavazzoni, D. Ceresoli, M. Cococcioni, et al., Advanced capabilities for materials modelling with Quantum ESPRESSO, J. Phys. Condens. Matter. 29 (2017), 465901 arXiv:1709.10010v1 [cond-mat.mtrl-sci].
[23] A. Dal Corso, Pseudopotentials periodic table: From H to Pu, Comput. Mater. Sci. 95 (2014) 337–350, https://doi.org/10.1016/j.commatsci.2014.07.043.
[24] K. Lee, É.D. Murray, L. Kong, B.I. Lundqvist, D.C. Langreth, Higher-accuracy van der Waals density functional, Phys. Rev. B - Condens. Matter Mater. Phys. 82 (2010), https://doi.org/10.1103/PhysRevB.82.081101.
[25] I. Píš, L. Ferrighi, T.H. Nguyen, S. Nappini, L. Vaghi, A. Basagni, E. Magnano, A. Papagni, F. Sedona, C. Di Valentin, S. Agnoli, F. Bondino, Surface-Confined Polymerization of Halogenated Polyacenes: The Case of Dibromotetracene on Ag (110), J. Phys. Chem. C. 120 (2016) 4909–4918, https://doi.org/10.1021/acs.jpcc.5b12047.
[26] L. Ferrighi, I. Píš, T.H. Nguyen, M. Cattelan, S. Nappini, A. Basagni, M. Parravicini, A. Papagni, F. Sedona, E. Magnano, F. Bondino, C. Di Valentin, S. Agnoli, Control of the intermolecular coupling of dibromotetracene on Cu(110) by the sequential activation of C-Br and C-H bonds, Chem. - A Eur. J. 21 (2015) 5826–5834, https://doi.org/10.1002/chem.201405817.
[27] A. Basagni, L. Ferrighi, M. Cattelan, L. Nicolas, K. Handrup, L. Vaghi, A. Papagni, F. Sedona, C. Di Valentin, S. Agnoli, M. Sambi, On-surface photo-dissociation of C-Br bonds: Towards room temperature Ullmann coupling, Chem. Commun. 51 (2015) 12593–12596, https://doi.org/10.1039/c5cc04317d.
[28] M. Smerieri, I. Píš, L. Ferrighi, S. Nappini, A. Lusuan, L. Vattuone, L. Vaghi, A. Papagni, E. Magnano, C. Di Valentin, F. Bondino, L. Savio, Synthesis of corrugated C-based nanostructures by Br-corannulene oligomerization, Phys. Chem. Chem. Phys. 20 (2018) 26161–26172, https://doi.org/10.1039/c8cp04791j.
[29] J.D.P. Hendrik, J. Monkhorst, Special points for Brillonin-zone integrations*, Phys. Rev. B. 13 (1976) 5188–5192, https://doi.org/10.1103/physrevb.13.5188.
[30] D.R. Tersoff, J. and Hamann,, Theory of the scanning tunneling microscope, Phys. Rev. B. 31 (1985) 805–813, https://doi.org/10.1103/PhysRevB.31.805.
[31] D. Nečas, P. Klapetek, Gwyddion: An open-source software for SPM data analysis, Cent. Eur. J. Phys. 10 (2012) 181–188, https://doi.org/10.2478/s11534-011-0096-2.
[32] G. Henkelman, B.P. Uberuaga, H. Jónsson, Climbing image nudged elastic band method for finding saddle points and minimum energy paths, J. Chem. Phys. 113 (2000) 9901–9904, https://doi.org/10.1063/1.1329672.
[33] L. Vattuone, D.A. King, Energetics of adsorption, Single Crystal Calorimetry, in: M. Rocca, T.S. Rhaman, L. Vattuone (Eds.), Springer Handb. Surf. Sci., Springer series in surface sciences, 2020: pp. 1005–1034. https://doi.org/https://doi.org/10.1007/978-3-030-46906-1.
[34] G.M. National Institute of Standards and Technology, NIST X-ray Photoelectron Spectroscopy Database, (2000). https://doi.org/doi:10.18434/T4T88K.
[35] F. Orlando, P. Lacovig, M. Dalmiglio, A. Baraldi, R. Larciprete, S. Lizzit, Synthesis of nitrogen-doped epitaxial graphene via plasma-assisted method: Role of the graphene-substrate interaction, Surf. Sci. 643 (2016) 214–221, https://doi.org/10.1016/j.susc.2015.06.017.
[36] R.H. Temperton, A.J. Gibson, K. Handrup, J.N. O'Shea, Adsorption and charge transfer interactions of bi-isonicotinic acid on Ag(111), J. Chem. Phys. 147 (5) (2017) 054703, https://doi.org/10.1063/1.4996746.
[37] R. Costantini, H. Ustunel, Z. Feng, M. Stredansky, D. Toffoli, G. Fronzoni, C. Dri, G. Comelli, D. Cvetko, G. Kladnik, G. Bavdek, L. Floreano, A. Morgante, A. Cossaro, Methylamine terminated molecules on Ni(1 1 1): A path to low temperature synthesis of nitrogen-doped graphene, FlatChem. 24 (2020), 100205, https://doi.org/10.1016/j.flatc.2020.100205.
[38] G. Bracco, A.C. Levi, Roughening Transition: Theories and Experiments, in: M. Rocca, T.S. Rhaman, L. Vattuone (Eds.), Springer Handb. Surf. Sci., Springer series in surface sciences, 2020: pp. 3–44. doi.org/10.1007/978-3-030-46906-1.
[39] T. Zambelli, J. Barth, J. Wintterlin, Formation mechanism of the O-induced added-row reconstruction on Ag(110): A low-temperature STM study, Phys. Rev. B - Condens. Matter Mater. Phys. 58 (1998) 12663–12666, https://doi.org/10.1103/PhysRevB.58.12663.
[40] B.E. Hayden, K.C. Prince, P.J. Davie, G. Paolucci, A.M. Bradshaw, Alkali metal-induced reconstruction of Ag(110), Solid State Commun. 48 (1983) 325–328, https://doi.org/10.1016/0038-1098(83)90732-9.
[41] R. Bernard, T. Leoni, A. Wilson, T. Lelaidier, H. Sahaf, E. Moyen, L. Assaud, L. Santinacci, F. Leroy, F. Cheynis, A. Ranguis, H. Jamgotchian, C. Becker, Y. Borensztein, M. Hanbücken, G. Prévot, L. Masson, Growth of Si ultrathin films on silver surfaces: Evidence of an Ag(110) reconstruction induced by Si, Phys. Rev. B - Condens. Matter Mater. Phys. 88 (2013) 2–6, https://doi.org/10.1103/PhysRevB.88.121411.